The Compact Muon Solenoid Experiment

CMS Note

Mailing address: CMS CERN, CH-1211 GENEVA 23, Switzerland

20 December 2006

Azimuthal anisotropy in Heavy Ions collisions with CMS Tracker

G. Kh. Eyyubova, V. L. Korotkikh, I. P. Lokhtin, S. V. Petrushanko, L. I. Sarycheva, A. M. Snirigev.

Scobeltsyn Institute of Nuclear Physics, Moscow State University, 119992 Moscow, Russia

Draft 4

Abstract

The azimuthal anisotropy of charge particles in Heavy Ions collisions is a very sensitive signature of QGP evolution at early stages. CMS tracker allows to measure the elliptic flow v_2 with high accuracy.

1 Introduction

The azimuthal anisotropy of charge particles is one of the most important features of the dense quark-gluon plasma (QGP) in heavy ions collisions. In non-central collisions of two nuclei the beam direction and the impact parameter define a reaction plane of each event. The observed particle yield versus azimuthal angle with respect to the event-by-event reaction plane gives information on the early collision dynamic [1],[2]. An initial overlap region has an "almond" form at non-zero impact parameter. If the produced matter interacts and thermalizes, pressure is built up within almond matter, generating anisotropic pressure gradients. This pressure pushes against the outside vacuum and the matter expands collectively. The expansion is the fastest along the largest gradient, i.e. along the shortest axis of the almond. The result is an anisotropic p_T distribution in the detected particles. One can expand this p_T distribution in a Fourier series. The second coefficient of the expansion v_2 is often called the elliptic flow and it is expected to be the dominant contribution.

The elliptic flow was measured at low and high energies (SPS-RHIC) (see Fig.1) ([7]). A ratio elliptic flow to spatial eccentricity archives the values of 0.2 at RHIC energies which is consistent with hydrodynamical limit.

In the RHIC experiments for $Au + Au$ collisions at 200A GeV [3],[7],[5]. $v_2(p_T)$ is increasing with p_T up to $p_T \simeq 1GeV/s$ and then it is saturated. This increasing and v_2 value are described by hydrodynamic model [6]. At higher $p_T > 1GeV/c$ it is necessary to introduce other model descriptions, including the energy loss of hard partons in dense medium. The change of regime in p_T dependence in the intermediate region coincides with the beginning of the jet saturation region. $v_2(\eta)$ dependence is also not described by hydrodynamic model. It has maximum at $\eta = 0$ and falls with increasing of $|\eta|$ in contrast to a approximately plateau in $|\eta| < 2$ in hydrodynamic model.

The capabilities of CMS calorimetric system to study elliptic energy flow are analyzed in [8]. It was shown that the calorimetric system is well suited to measure energy flow and jet azimuthal anisotropy at high p_T.

But it is more actual to study the capabilities of CMS tracker to measure the particle azimuthal anisotropy in the intermediate p_T region.

2 The CMS Tracker

2.1 Geometrical layout

The tracker is located, together with the electromagnetic and hadronic calorimeters, inside a 4 T solenoidal magnetic field. It consists of a pixel detector, providing 2 to 3 hits per track, and Silicon Strip detector providing 10 to 14 hits. There are about 10 million microstrips and 40 million pixels.

The pixel detector is composed of 3 cylindrical layers and 2 pairs in the end-caps, such that 3 points are measured per track for $|\eta| < 2.2$. In the barrel, the three layers are located at radii of 4.3 cm, 7.5 cm, 10.2 cm, and in the end-caps the two pairs of disks are located at $|z| = 34.5$ cm, $|z| = 46.5$ cm. With the pixel size of $100 \times 150\mu m$ the hit resolution is approximately of 10 μm in $r - \varphi$, and 20 μm in $r - z$.

The Silicon Strip detector has the following parts. The Inner Barrel (TIB) is composed of 4 cylindrical layers, enclosed by 3 pairs of disks (Inner Disks, TID). It is then followed by 6 cylindrical layers of the Outer Barrel (TOB). The End-Caps (TEC) are made of 9 pairs of disks. Strip length range from 9 cm in the inner part to 21 cm in the outer part, and pitches range from 80 to 205 μm. Some of the layers and rings of disks are instrumented with double sided modules, where the detectors are glued back-to-back with a stereo angle of 100 mrad.
The schematic layout and geometrical coverage of the tracker is shown in Fig.2.

2.2 Track reconstruction

The baseline algorithm for track reconstruction [11] in CMS is the Combinatorial Kalman Filter. After track hits have been reconstructed the track reconstruction proceeds the following four steps: trajectory seeding, pattern recognition, trajectory cleaning, track fitting and smoothing.

Kalman filter proceeds iteratively from the seed layer and includes the information of the successive acceptable layers one by one. With each included layer, track parameters are better constrained. In the extrapolation of the trajectory from layer to layer, the effects of energy loss and multiple scattering are accounted for.

The global track finding efficiency in p-p collisions for muons is about 98% over most of the tracker acceptance. For hadron the efficiency is between 75 and 95% ([12]). For nucleus-nuclear collisions the efficiency is lower

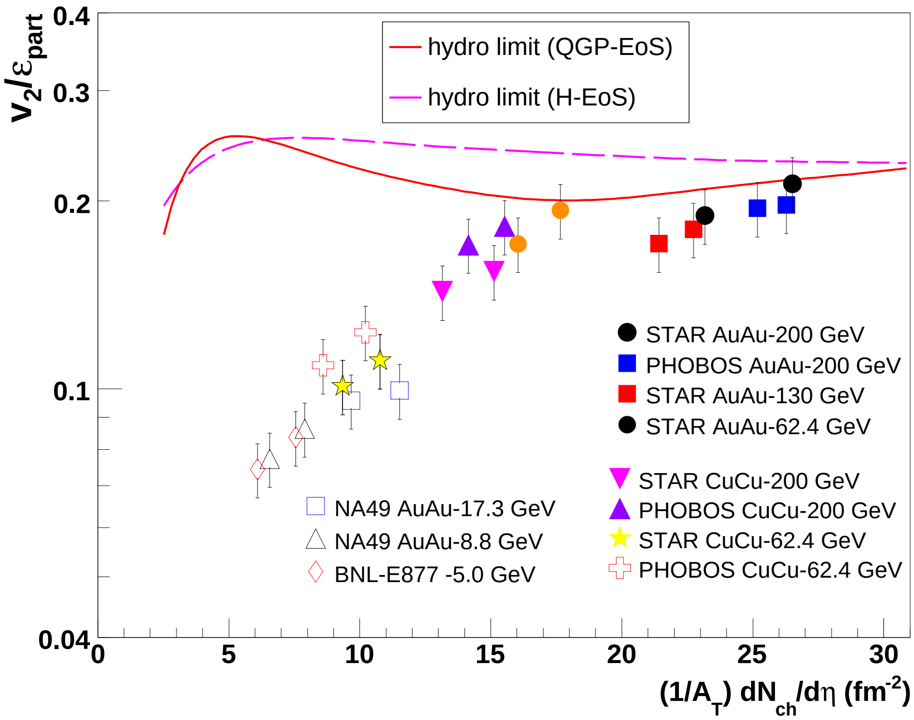

Figure 1: A ratio elliptic flow to spatial eccentricity as a function of the hadron rapidity density normalized by the reaction overlap area $A_\perp$, compared to the hydrodynamical limit for a fully thermalized system with QGP or hadron EoS. Figure is taken from [10]

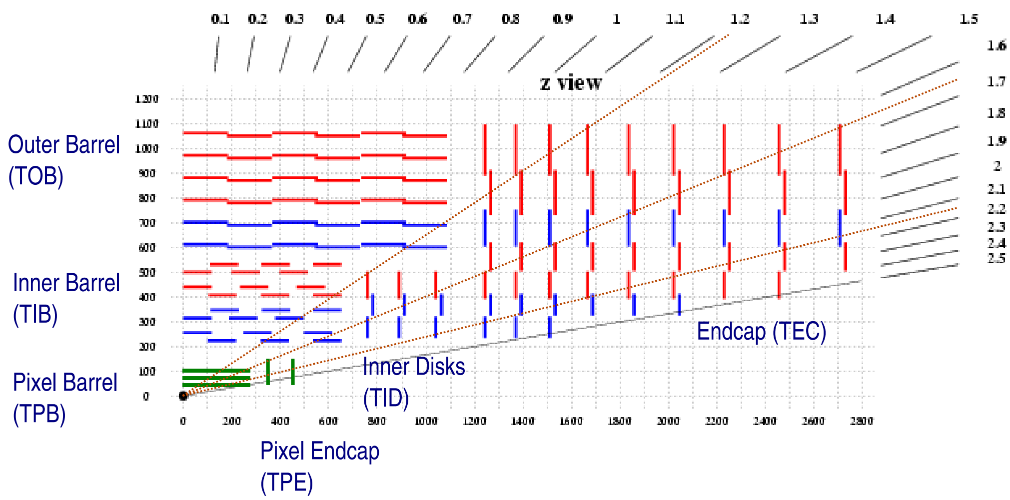

Figure 2: Illustration of the CMS Tracker layers, one quarter of the full tracker in rz view.

(70% - 80%) because of high multiplicity and large number of fake tracks ([13]).

3 Reconstruction of charge particle distributions

This study is based on simulations of heavy ion collisions using HYDJET event generator [**?**]. A sample of 1000 Pb-Pb events at impact parameter $b = 9$ fm was utilized. At these centralities the full multiplicity in one event is about 200 - 300. Some settings were used to reconstruct tracks (the number of hits on a track > 12, the track fit probability > 0.01) and a cut on $p_T > 0.9$ GeV was set in both simulated and reconstructed events.

3.1 Multiplicity

The azimuthal charge particle distribution for 1000 simulated and reconstructed events is shown in Fig3, the reaction plane angle in the simulated events was equal to zero (see Fig. 3).

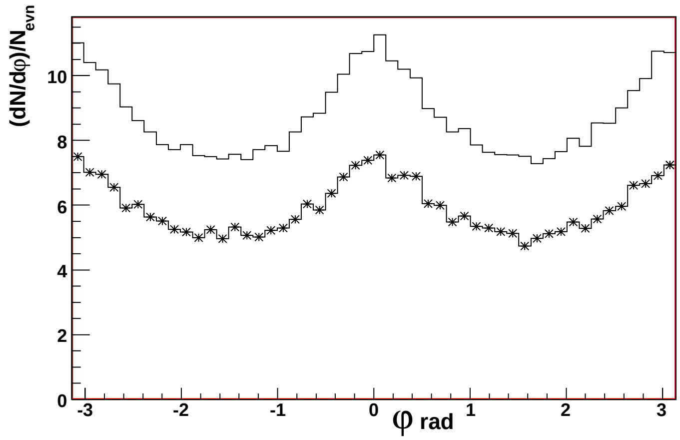

Figure 3: Simulated and reconstructed(red) particle distribution at impact parameter b=9 fm, 1000 events

An anisotropic azimuthal pattern is seen at generated and track reconstructed levels.

Also we show here the p_T- and $\eta-$ charge particle distribution for simulated and reconstructed events at Fig4.

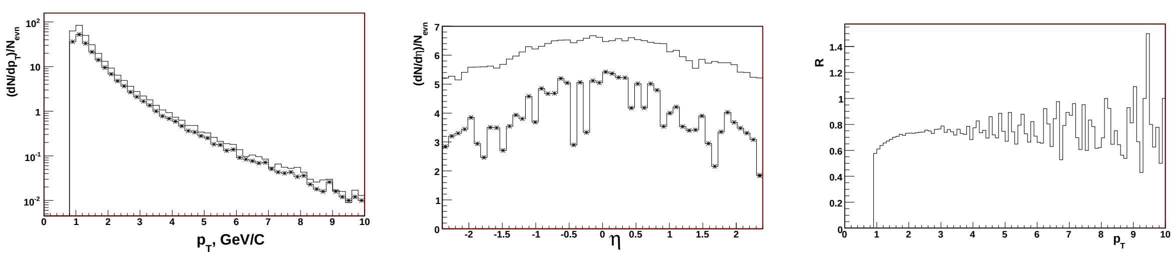

Figure 4: a)p_T- distribution of rec and sim events, b)η- distribution c) Ratio of reconstructed and simulated p_T-distribution at impact parameter b=9 fm, 1000 events

3.2 Reconstruction of nuclear reaction plane

To determine the reaction plane we use here the method suggested in [8]:

$$\tan n\psi_n = \frac{\sum_i w_i \sin(n\varphi_i)}{\sum_i w_i \cos(n\varphi_i)} \tag{1}$$

where φ_i is the azimuthal position of the i-th particle, w_i is the weight, and the sum runs over all particles.

The accuracy of event plane determination is mainly sensitive to two model factors: the strength of elliptic flow, and the event multiplicity. A set of 1000 HYDJET Pb+Pb events for each centrality bin covering the range of impact parameters from $b = 0$ to $b = 2R_A$ (R_A is a nuclear radius) without jet quenching was used. Stable particles with pseudorapidity of $|\eta| < 3$ (CMS barrel+endcap calorimetry acceptance) were considered for event plane analysis with the method (**??**) for $n = 2$ and $\omega_i = p_{Ti}$. An additional cut $p_T^{\rm ch} > 0.8$ GeV/c on charged particle transverse momentum was applied in order to take into account the effect of charged particles with smaller p_T values. Such particles cannot reach the calorimeter surface in the 4 T CMS magnetic field.

Figure 5 shows the calculated resolution $\sigma(\Psi_0)$ (which is defined as the width of Gaussian fit of the distribution over the difference between the generated and reconstructed azimuthal angle of the reaction plane) as a function

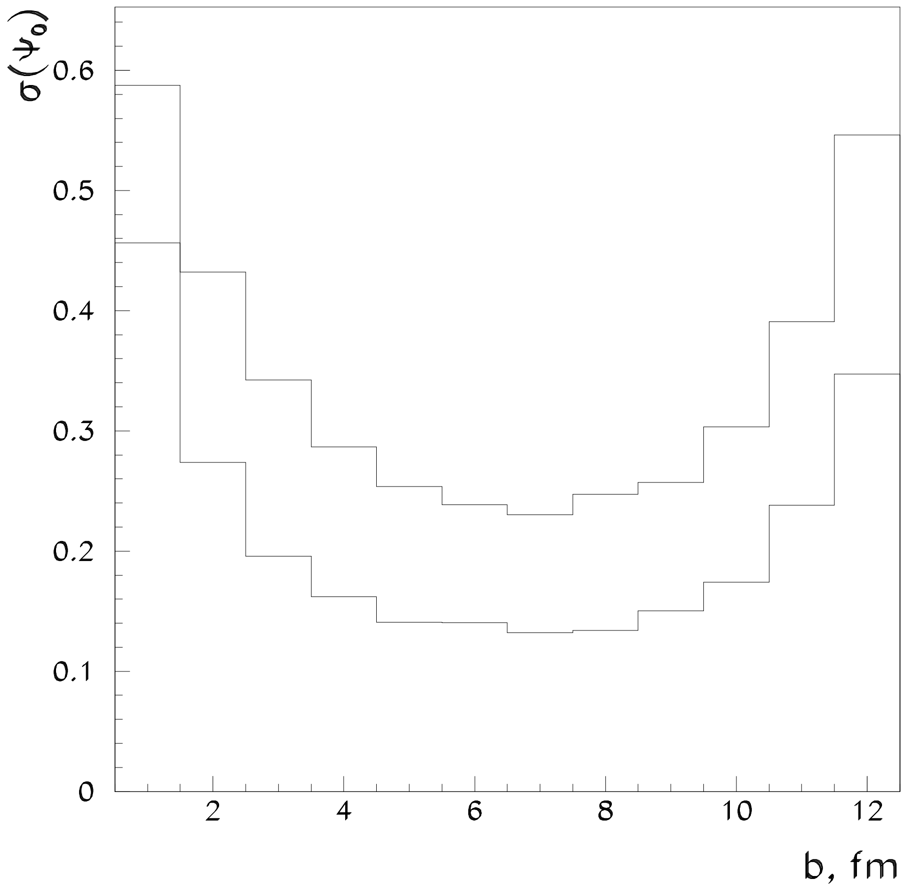

Figure 5: Event plane resolution $\sigma(\Psi_0)$ as a function of impact parameter in Pb+Pb collisions with "standard" (solid histogram) and "high" (dashed histogram) multiplicities.

of impact parameter in Pb+Pb collisions. The interplay of multiplicity and anisotropic flow in opposite centrality directions results in the best resolution obtained in semi-central collisions. Here, semi-central collisions have an impact parameter on the order of the nuclear radius, $b \sim R_A$. In order to demonstrate the influence of multiplicity on the accuracy of event plane determination, the resolution for "high" multiplicity events (obtained by increasing the multiplicity of the soft part of the event by a factor of 2, i.e. with the total multiplicity of soft part ~ 52000 in central Pb+Pb collisions) was also calculated. Increasing the soft multiplicity by a factor of 2 results in an improvement of resolution by a factor ~ 1.7 with a rather weak dependence on the event centrality.

Introducing jet quenching into the model results in a rise of event multiplicity and the generation of some additional elliptic flow in the high-p_T region. The estimated improvement on the event plane resolution in this case is on the level of 20-25% for "standard" and "high" multiplicities.

The distributions of reaction plane angle $\Psi_R = \Psi_2$, obtained by (1) for $n = 2$ and $w_i = 1$ are shown in Fig6a and Fig6b. The resolution of angle for simulated events is equal to $\sigma_{sim} = 0.27$. The resolution with CMS Tracker is better than that of CMS calorimeters [**?**]. Comparison of two resolutions see in Table 1). .

Table 1: Resolution of reaction plane reaction.

Detector	σ_{rec}
ECAL+HCAL(Barrel+Endcaps)	0.37
Tracker	0.31

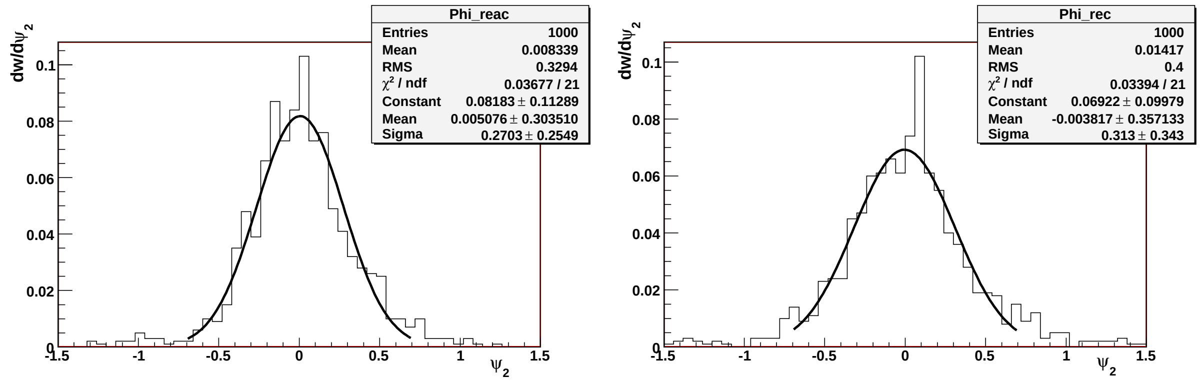

Figure 6: Distribution of the event plane angle for simulated (left) and reconstructed (right) events

4 v_2 calculation

We assume (according to hydrodynamic model) that in the expansion of particle distribution in a Fourier series the v_2 terms has the dominant contribution and the azimuthal distribution is described by the elliptic form:

$$\frac{dN}{d\varphi} = \frac{N_0}{2\pi}[1 + 2v_2 \cos 2(\varphi - \Psi_R)] \tag{2}$$

where Ψ_R is the event plane angle, N_0 stands for full multiplicity. Then v_2 is the average (over particles) of $\cos(2(\varphi - \Psi_R))$:

$$v_2 = < \cos(2(\varphi - \Psi_R)) > \tag{3}$$

Here we apply two methods to calculate v_2-coefficient. The first one uses the reaction plane angle determination mentioned above. The second one does not involve the event plane angle determination. The basic idea of the latter is that v_2 coefficient expressed in terms of particle correlations. Two methods give the equivalent result for v_2.

4.1 v_2 with known reaction plane angle

With known reaction plane angle the distributions of flow v_2 by formula (1) were made.

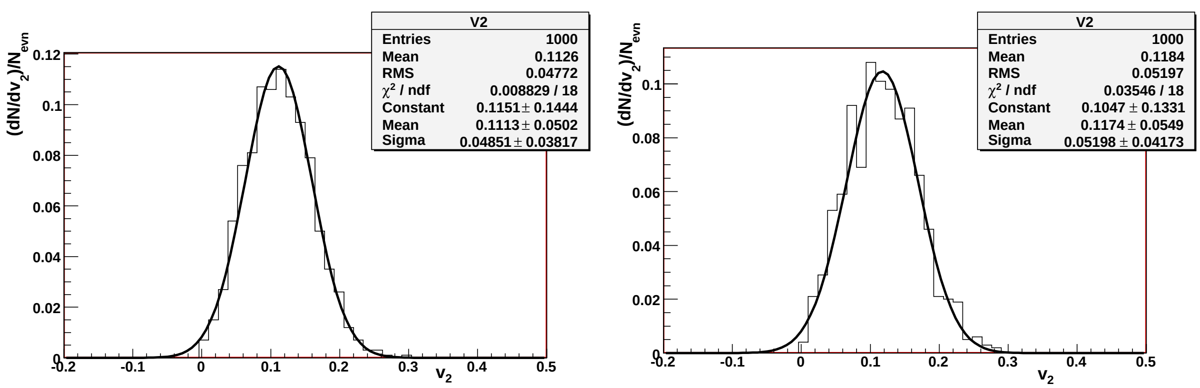

Figure 7: Distribution of v_2-coefficient in simulated (left) and reconstructed event (right) with reaction plane angle obtained by (1)

Results are in Fig. 10. The variance of v_2 is in Table 2.

4.1.1 p_T and η dependence

The p_T and η dependance of the elliptic flow are shown in Fig.8 and Fig.9.

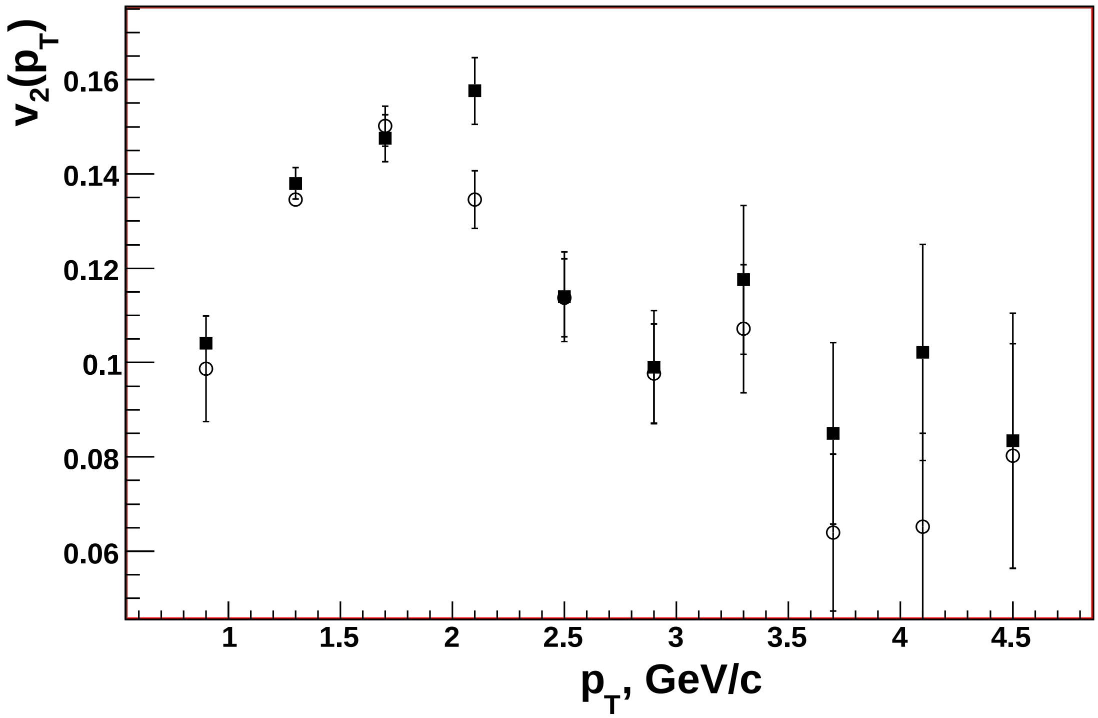

ht

Figure 8: p_T dependance. Cubes are reconstructed values of v_2, open points are simulated values of v_2

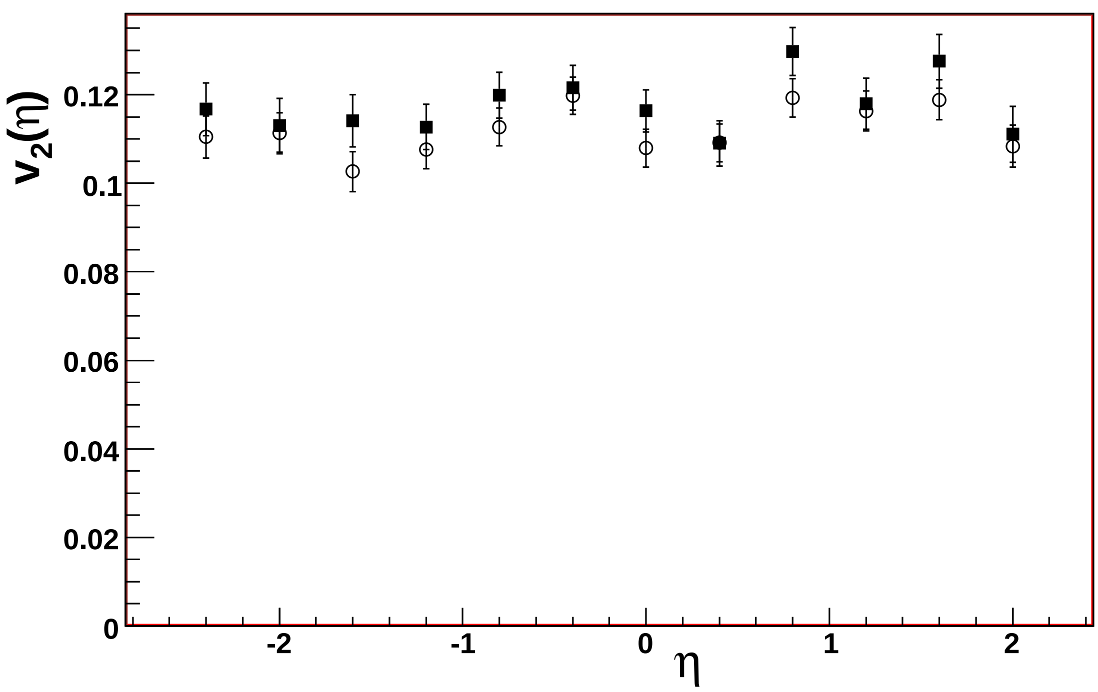

ht

Figure 9: η dependance. Cubes are reconstructed values of v_2, open points are simulated values of v_2

4.2 v_2 calculation by particle correlation

The method of v_2 calculation without event plane angle reconstruction was suggested in [9]. In the case then there are no other particle correlations except those due to flow, the coefficient of azimuthal anisotropy can be determined using a two-particle azimuthal correlator

$$v_2^2 =< \cos 2(\varphi_1 - \varphi_2) > \tag{4}$$

The variance of v_2 is in Table 2. A comparison of two method (3) and (4) is shown for a ratio v_2^{rec}/v_2^{sim}. Coefficient v_2 with reconstructed events by CMS Tracker differs on % 5 from simulated events for two methods.

This ratio is larger than unit because we lost the events at $0.9 < p_t \leq 1.1 GeV$ on level of reconstruction. This region has large values of multiplicity (see Fig. 4) and smaller v_2 magnitudes.

///////////////////

Also we show here the v_2 distribution, extracted from fitting of $dN/d\varphi$-distribution by fomular (2) with free parameters N_0, v_2 and Ψ_R.

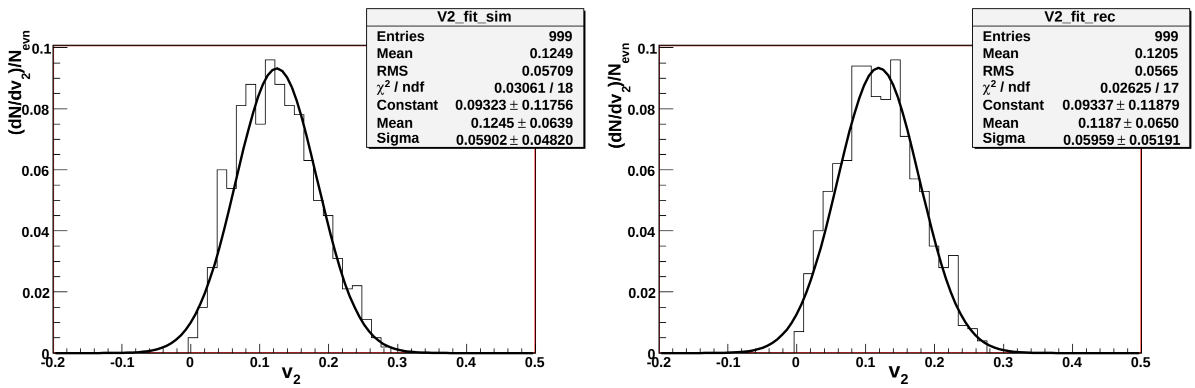

Figure 10: Distribution of v_2-coefficient in simulated (left) and reconstructed event (right)from fitting by fomular (2)

Table 2: Ratio of v_2 for reconstructed and simulated events and v_2 variance.

Method	v_2^{rec}	$\sigma(v_2)$	v_2^{rec}/v_2^{sim} at the same p_T cut	v_2^{rec}/v_2^{sim} at not equal cuts
$< \cos 2(\varphi - \Psi_R) >$	0.1184	0.051	1.055	XXXX
$\sqrt{(< \cos 2(\varphi_1 - \varphi_2) >)}$	0.1184	0.052	1.055	XXXX
v_2 from fitting	0.1187	0.059	0.95	xxxx

5 Conclusion

The azimuthal flow was calculated here by two methods. It was shown that these two methods give similarly results, because they are based on the same suggestion that the azimuthal distribution of particles is described by the elliptic form.

The resolution of reaction plane angle is better with CMS tracker than with calorimeters.

References

[1] J.-Y. Ollitrault, Phys. Rev. **D46**, 229 (1992).

[2] H. Sorge, Phys. Rev. Lett. **82**, 2048 (1999).

[3] K. Adcox et al.(PHENIX), Nucl. Phys. **A757**, 1 (2005).

[4] B. Back et al.(PHOBOS), Nucl. Phys. **A757**, 28 (2005).

[5] J. Adams et al.(STAR), Nucl. Phys. **A757**, 102 (2005).

[6] P. Huovinen et al., Phys. Lett. **B503**, 58 (2001).

[7] S. Mainly (PHOBOS Collaboration), Nucl. Phys. **A774**, 523 (2006).

[8] I.M. Lokhtin et al., CMS Nore 2003/019, 2003..

[9] I. P. Lokhtin, L. I. Sarycheva and A. M. Snigirev, "Extracting the jet azimuthal anisotropy from higher order cumulants," Eur. Phys. J. C **30** (2003) 103 [arXiv:hep-ph/0304009].

[10] D. d'Enterria, arXiv:nucl-ex/0611012.

[11] W. Adam et al., Track reconstructiom in the CMS Tracker, CMS Note 2006/041 (2006).

[12] F. -P. Shilling (CMS Collaboration), arXiv:physics/0610005, 2006

[13] G. Roland,Track Reconstruction in HI Events using the CMS Tracker, CMS Note 2006/031 (2006)